Journal of Solid State Chemistry 183 (2010) 2382–2388

Contents lists available at ScienceDirect

Journal of Solid State Chemistry

journal homepage: www.elsevier.com/locate/jssc

Simple synthesis of ultra-long Ag_2Te nanowires through solvothermal co-reduction method

Feng Xiao, Gang Chen *, Qun Wang, Lin Wang, Jian Pei, Nan Zhou

Department of Applied Chemistry, Harbin Institute of Technology, Harbin 150001, People's Republic of China

ARTICLE INFO

Article history:
Received 11 March 2010
Received in revised form
27 May 2010
Accepted 12 July 2010
Available online 17 July 2010

Keywords:
Silver telluride
Solvothermal
Nanowires
Electrical transport property

ABSTRACT

Ultra-long single crystal β-Ag_2Te nanowires with the diameter of about 300 nm were fabricated through a solvothermal route in ethylene glycol (EG) system without any template. The long single crystal wires were curves, with high purity, well-crystallized, and dislocation-free and characterized by using X-ray powder diffraction (XRD), Differential scanning calorimetry (DSC) analysis, X-ray photoelectron spectroscope (XPS), field emission scanning electron microscopy (FE-SEM), transmission electron microscopy (TEM) and high-resolution transmission microscopy (HRTEM). The detailed topotactic transformation process from particles into single crystal wires was studied. Furthermore, the electrical conductivity and Seebeck coefficient have been systematically studied between 300 and 600 K.

1. Introduction

Metal tellurides have drawn considerable attention because of their unique physical properties and potential applications in fabricating sensors for detection of low energy gamma-ray detection [1], low-dimensional phase-change nanomaterials for information storage [2,3], thermoelectric materials [4,5], field sensing devices, etc. [6]. Among these tellurides, silver tellurides are a series of compounds with variable stoichiometries, and the four typical stable silver telluride phases are AgTe [7,8], Ag_2Te [9], Ag_5Te_3 [10], and Ag_7Te_4 [11]. These silver telluride materials may find applications in manufacture of magnetic field measurements [12–15], memory devices [16], and optics materials [17]. Recently, silver telluride (Ag_2Te) has received great attentions due to its interesting and useful characteristics [18]. The low-temperature phase of monoclinic silver telluride is a kind of semiconductor with a narrow band gap, high carrier mobility, and low lattice thermal conductivity, whereas its high-temperature phase gives rise to superionic conductivity because Ag^+ cations can easily move through the cubic sublattice formed with tellurium anions [19,20].

Generally, Ag_2Te bulk material was prepared by the solid reaction between elemental Ag and Te at elevated temperature in evacuated tubes [21], or by the aqueous reaction of metal–salt solutions with toxic gaseous H_2Te [22]. Recently, low-dimensional nanostructures, including nanowires, nanorods, and nanosheets, are of importance because they exhibit promising mechanical, electrical, optical, and magnetic properties different from those of corresponding polycrystalline powders. A number of methods for the synthesis of Ag_2Te with nanostructures have been explored. For example, Ag_2Te nanowires were obtained by cathodic electrolysis from dimethyl sulfoxide (DMSO) solution containing $AgNO_3$ and $TeCl_4$ in porous anodic alumina membranes [20]. Ag_2Te nanorods were prepared by the reaction between AgCl and elemental Te in the mixed solvent of ethylenediamine and hydrazine hydrate [23]. A room-temperature solution-phase route for the preparation of one-dimensional silver telluride nanowires (Ag_2Te NWs) has been reported [24]. Silver telluride nanotubes have been prepared by the solvothermal process without a template or a surfactant [25]. Template-engaged method in which the Te nanorods were used as template reagents has been developed for the synthesis of the Ag_2Te nanorods [26]. However, most objects of these syntheses have to use templates which served as a physical scaffold and hard to obtain long wires ($>20\,\mu m$ in length). Herein, we have developed a general strategy to grow large scale, ultra-long Ag_2Te nanowires through solvothermal co-reduction method without any template. Moreover, the formation mechanism of the nanostructured silver telluride has been elucidated on the basis of the experimental observations.

2. Experimental section

2.1. Synthesis

Ultra-long Ag_2Te nanowires were prepared from $AgNO_3$ (99.99%) and Na_2TeO_3 (99.98%) by a solvothermal co-reduction

* Corresponding author. Fax: +86 451 86413753.
E-mail address: gchen@hit.edu.cn (G. Chen).

0022-4596/$ - see front matter Crown Copyright © 2010 Published by Elsevier Inc. All rights reserved.
doi:10.1016/j.jssc.2010.07.020

method. In a typical experiment, the aqueous solutions of 0.2208 g $AgNO_3$ (1.3 mmol) and 0.2215 g Na_2TeO_3 (1 mmol) were prepared by adding 5 mL deionized water. 1 g (2.68 mmol) disodium salt of ethylenediaminetetraacetic acid ($Na_2(EDTA)\cdot 2H_2O$) was added into the solution of $AgNO_3$. After a vigorous stirring of 5 min, they were transferred into Teflon lined stainless steel autoclave of capacity 40 mL in sequence. Then 10 mL 1 M NaOH and 5 mL ethylene glycol (EG) were added immediately, which result in a few brownish-black spots floating on the surface of the mixed solution and the white milky liquid could be obtained by vigorous stirring. The final volume of the solution mixture was adjusted to 30 mL with deionized water and the autoclave was heated at 513 K. After 24 h, the vessel was taken out and allowed to cool to room temperature naturally, and the black cloudy precipitate found inside the autoclave was separated by centrifugation, washed with deionized water and ethanol several times, and dried in a vacuum at 323 K for 10 h. Moreover, the experimental conditions with different reaction time were also investigated in order to understand the growth mechanism of the ultra-long single crystal Ag_2Te wires. Table 1 summarizes these typical conditions and the corresponding morphologies and phases evolution of the products.

2.2. Characterization

X-ray diffraction data were collected at ambient temperature from 5° to 90° with a step of 0.02° on Rigaku D/max diffractometer working with Cu$K\alpha$ radiation. Differential scanning calorimetry (DSC) analysis was carried out up to a temperature of 500 K, using a SETARAM DSC-141 under a stream of nitrogen and a heating rate of 10 K/min. The XPS spectra were collected on an American Electronics physical PHI5700ESCA system, X-ray photoelectron spectroscope using Al$K\alpha$ radiation (1486.6 eV). The source was operated at 12.5 kV and the anode power was 250 W. The binding energy (BE) was calibrated with the C 1*s* peak. The morphology of particles was studied by field emission scanning electron microscopy (FE-SEM, FEI QUANTA 200F). Transmission electron micrographs were obtained by employing an FEI Tecnai G2 S-Twin transmission electron microscope, using an accelerating voltage of 300 kV. The powder specimens were prepared in air. Rectangular shape specimens of about $15.7\times 4.6\times 0.7$ mm^3 were obtained under a pressure of 15 MPa. The measurements of the electrical conductivity and Seebeck coefficient were carried out using a laboratory-designed apparatus under an argon atmosphere. The electrical conductivity of the samples were measured by four probe method with the increase in temperature of about 2.5 °C/min. For the measurement of Seebeck coefficient, thermo-electromotive force measured as a function of temperature gives a straight line and its slope is Seebeck coefficient. The detailed procedure for the measurement of Seebeck coefficient is described below. The sample with a pair of Pt/Rh thermocouples attached to two ends (bar-shaped sample) was heated to a certain temperature, and then one of the ends was heated by an extra thermal source to produce the temperature gradient; the temperature and voltage signals were collected by a commercial data acquisition system (Keithley 2700, Keithley Instruments Inc., America).

3. Results and discussion

3.1. Structure, formation, and morphology

The crystallinity of as-prepared samples was analyzed using X-ray diffraction (XRD) as shown in Fig. 1. It reveals that the product is composed of monoclinic Ag_2Te, which is consistent with those of bulk monoclinic Ag_2Te [space group: $P2_1/c$ (no. 13)] (JCPDS 34-0142). The calculated lattice constants $a=8.1586$ Å, $b=8.9339$ Å, and $c=8.0100$ Å were in agreement with the standard literature. No other diffraction peaks were detected such as Ag or Te crystalline phases. From the results of XRD, it can be concluded that high purity of Ag_2Te was obtained by the present synthetic method. In addition, Brownish-black Ag_2O which resulted from unstable intermediate product AgOH can be obtained in alkaline solution [27]. On the other hand, there was a strong complexing action between silver (I) ions and EDTA. So the black spots may be Ag_2O phase and the brownish-black precipitate disappeared because of the strong complexing action between silver (I) ions and EDTA.

To understand the chemical situation of elements in the product, the XPS test was performed, and the results are shown in Fig. 2. It can be found that a little oxides and carbon are present on the surface of the product. The oxides may result from the surface oxidation reaction of the Ag_2Te nanowires with O_2 [26]. The binding energies obtained from the XPS spectrum are 367.7 and

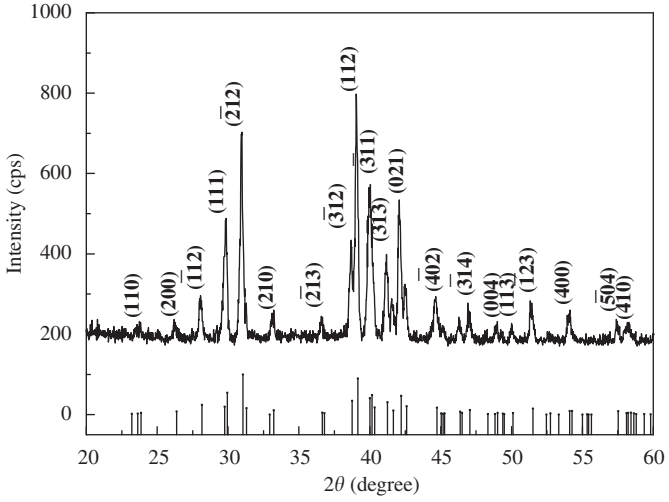

Fig. 1. The XRD pattern for Ag_2Te sample prepared at 513 K for the mol ratio of Ag/Te = 1.30.

Table 1
Summary of the synthesis of typical products under various experimental parameters.

Sample	*T* (K)	*t* (h)	Phase	Morphology
Sample1	513	2	Ag and Ag_2Te	Straight nanotubes and particles
Sample2	513	6	Ag, Te, and Ag_2Te	Straight nanotubes and particles
Sample3	513	8	Ag_2Te, Ag, and Te	Straight nanotubes, bent wires, and particles
Sample4	513	12	Ag_2Te, Te, and Ag	Straight nanotubes, bent wires, and particles
Sample5	513	16	Ag_2Te, Te, and Ag	Straight nanotubes, bent wires, and particles
Sample6	513	20	Main Ag_2Te	Bent wires and particles
Sample7	513	24	Pure β-Ag_2Te	Bent wires

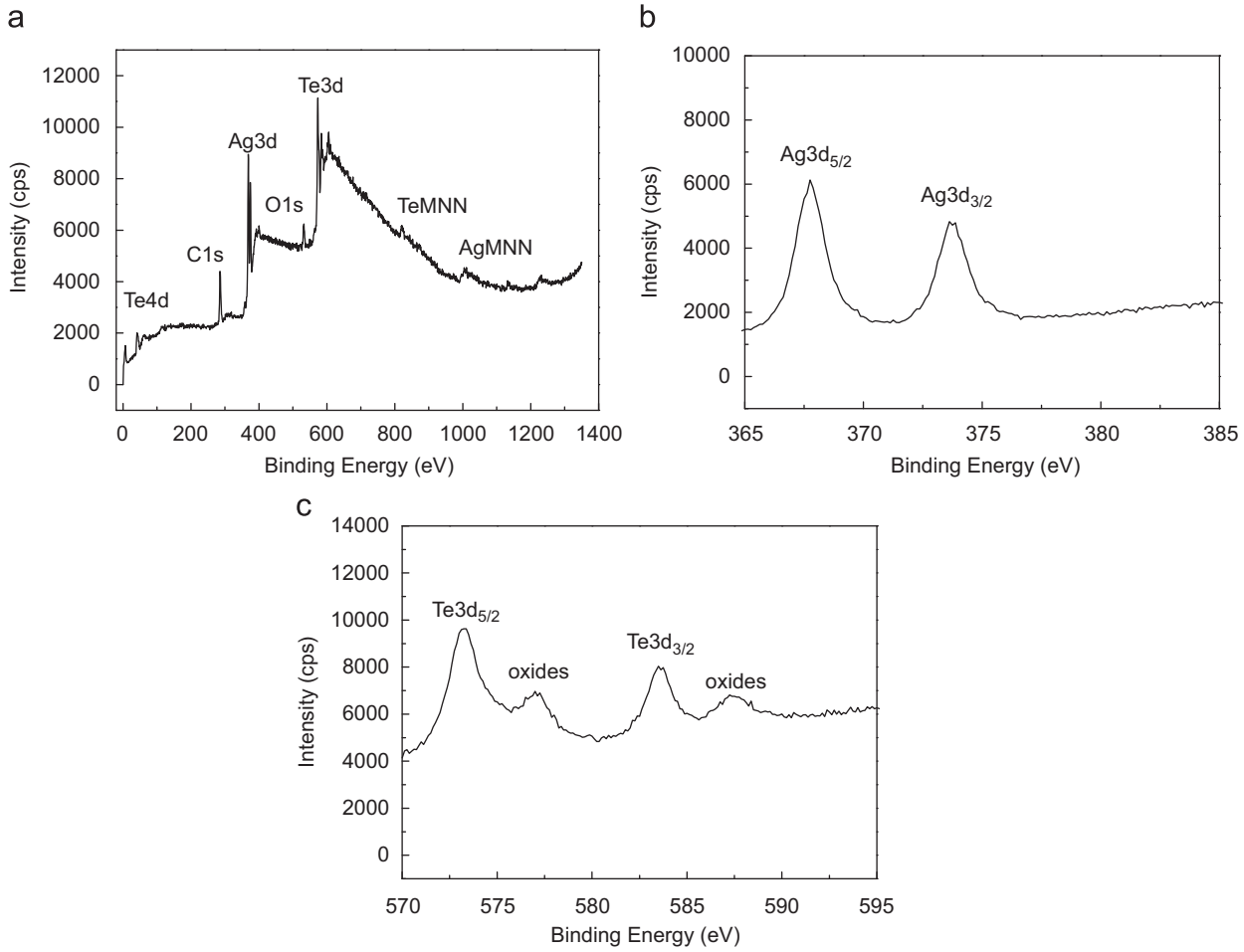

Fig. 2. XPS spectrum of the as-prepared pure Ag_2Te sample: (a) the survey spectrum, (b) narrow spectrum for Ag 3*d*, and (c) narrow spectrum for Te 3*d*.

573.3 eV for Ag $3d_{5/2}$ and Te $3d_{5/2}$ in Fig. 2a, respectively, which means that the product is composed of Ag (I+) and Te (II−). The peaks at 367.7 and 373.7 eV correspond to Ag $3d_{5/2}$ and Ag $3d_{3/2}$, respectively (Fig. 4b), and those at 573.3 and 583.5 eV correspond to Te $3d_{5/2}$ and Te $3d_{3/2}$, respectively (Fig. 4c). In addition, two small peaks are observed at 577.1 and 587.5 eV, which can be attributed to Te(IV) oxide. According to the quantification of XPS peaks, the molar ratio of Ag to Te is 2.05:1.00.

Morphological features of the samples were investigated by FE-SEM as shown in Fig. 3. The low-magnification FE-SEM image (Fig. 3a) reveals that the typical products consist of a large quantity of wire-like structures with the lengths in the range of several tens to several hundred micrometers. The high-magnification FE-SEM image (Fig. 3b) shows that the diameter of wire-like structures is 300−500 nm. To the best of our knowledge, the synthesis of ultra-long silver telluride nanowires have never previously been reported.

In order to further understand the morphology and microstructure of the wire-like Ag_2Te, a detailed investigation was performed using high-resolution TEM (HRTEM). Fig. 3c shows the low-magnification TEM image of a single ultra-long Ag_2Te wire with diameters between 200 and 400 nm, lengths ranging from 8 to 10 μm. In addition, from the TEM iamge, we found that the ultra-long silver telluride wires can be destroyed by ultrasound during the TEM sample preparation. Fig. 3d shows a typical HRTEM image of a single nanowire and reveals the single-crystalline nature of the nanowires, and free of dislocation. The interplanar spacing of 0.372 and 0.685 nm are consistent with the (1 1 0) and (1 0 0) plane of Ag_2Te. Moreover, the FFT pattern (left inset in Fig. 3d) further substantiates that the Ag_2Te nanowire is a monoclinic phase.

A series of experiments were carried out to study the influence of the ratio of $AgNO_3$ to Na_2TeO_3 and $Na_2(EDTA)\cdot 2H_2O$ as well as NaOH on the synthesis of products. It can be seen in Fig. 4a–d that the phases in the samples prepared at 513 K for different ratios of $AgNO_3$ to Na_2TeO_3 are composed of monoclinic phase Ag_2Te (JCPDS: 34-0142) and Ag (JCPDS: 04-0783) or Te (JCPDS: 65-3370). As the ratio of $AgNO_3$ to Na_2TeO_3 decreases, the amount of the Ag phase decreases gradually, then Te phase appears (Fig. 4d). Here another point to be noted is that pure Ag_2Te shown in Fig. 1 is for the ratio 1.30. It means that the ratio of 1.30 for $AgNO_3$ to Na_2TeO_3 is required for the preparation of pure long wire Ag_2Te under solvothermal synthesis at 513 K. In addition, $Na_2(EDTA)\cdot 2H_2O$ and NaOH played a key role in this solvothermal co-reduction process. It can be seen in Fig. 4e and f that the phases Ag_7Te_4 (JCPDS: 18-1187) and Ag (JCPDS: 04-0783) appeared in the samples prepared at 513 K and Ag/Te = 1.30 for 24 h in the absence of NaOH and $Na_2(EDTA)\cdot 2H_2O$, respectively. First of all, the pH value played an important role during this reaction, which influenced on the purity of samples. Ag_7Te_4 phase would appear without NaOH added, which implied that NaOH could influence the reaction greatly. A branch reaction for elemental Te would occur in an alkaline environment to form both positive ions (Te occurs as +4 valence in TeO_3^{2-}) and negative ions (Te^{2-}) simultaneously [28]. The disproportionation of a little Te in alkaline environment may be essential for the purity of samples. There would be a little surplus Te to produce Ag_7Te_4 phase without the disproportionation. On the other hand, $E_{Ag+/Ag}$

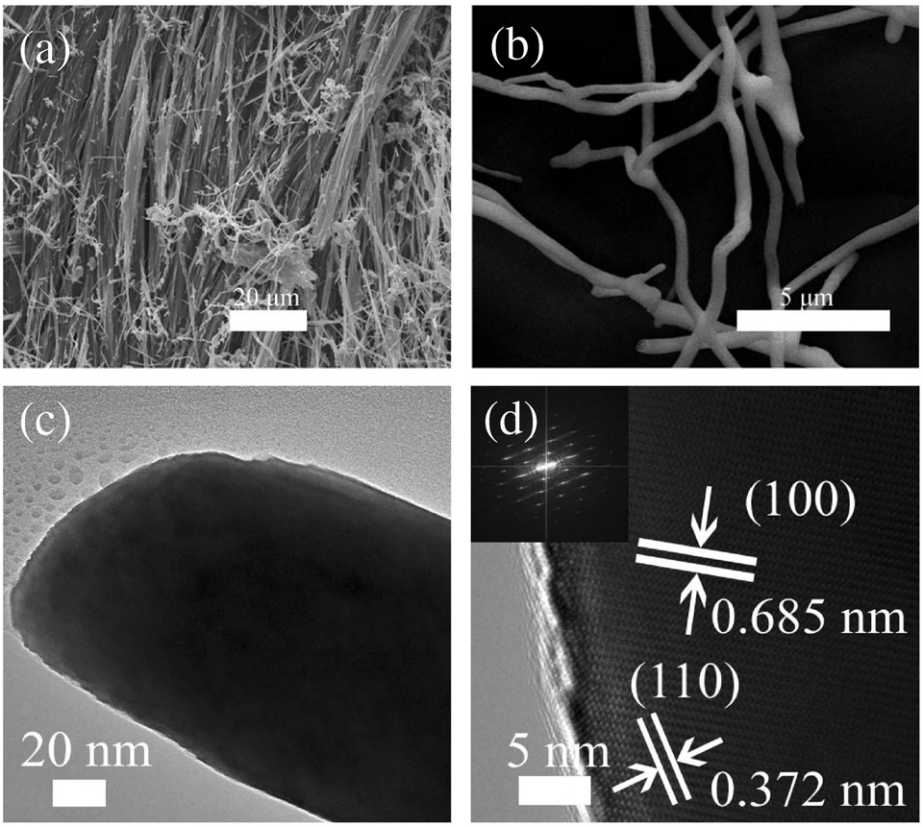

Fig. 3. SEM images of the as-prepared Ag_2Te samples synthesized at 513 K for 24 h with 1.30 (a) and (b) for the ratio of $AgNO_3$ to Na_2TeO_3, (c) TEM image of the Ag_2Te wire. (d) HRTEM image recorded on the edge of this wire. Inset: FFT image of the HRTEM image (left).

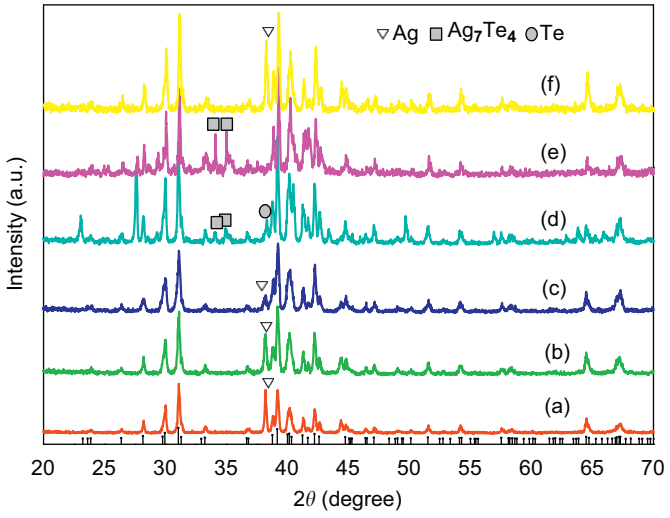

Fig. 4. The XRD patterns for Ag_2Te samples for (a) Ag/Te=1.70, (b) Ag/Te=1.58, (c) Ag/Te=1.44, (d) Ag/Te=1.00, and Ag/Te=1.30 for (e) no NaOH and (f) no $Na_2(EDTA)\cdot 2H_2O$.

was so high [29] to produce Ag phase easily in a short time that it could not react with Te phase completely which was produced relatively slowly. Consequently, pH value could adjust $E_{Ag^+/Ag}$ to a proper value in order to obtain a pure phase. Similarly, Batabyal and Vittal [16] has approved that the pH value influenced the Ag^+ reduction. Then, the role of $Na_2(EDTA)\cdot 2H_2O$ was also investigated. Sample S2 which contained both Ag phase and Ag_2Te phase was obtained when no $Na_2(EDTA)\cdot 2H_2O$ was added. $Na_2(EDTA)\cdot 2H_2O$ played a critical role in the formation of the Ag_2Te nanowires. $Na_2(EDTA)\cdot 2H_2O$ could not only stabilize Ag^+ at the beginning stage, but also release Ag^+ gradually when main reaction consumes Ag phase. In aqueous solution, the strong complexing action between silver (I) ions and $Na_2(EDTA)\cdot 2H_2O$ resulted in the formation of Ag-EDTA complexes. The formation of the complexes could reduce the concentration of free Ag^+ in the solution, and slow the reaction rate, which is favorable for the growth of Ag_2Te nanowires. While if no $Na_2(EDTA)\cdot 2H_2O$ was added, Ag^+ would be quickly reduced by EG at 240 °C, which resulted in Ag impurity in samples [30].

It is known that silver telluride exhibits a structural phase transition from low-temperature monoclinic phase (α-Ag_2Te) to cubic phase (β-Ag_2Te) [18]. DTA, TG, and DSC analyses have been carried out to determine transformation temperature of our sample and to apply to subsequent test of electrical conductivity and Seebeck coefficient, and the results are shown in Fig. 5a. A distinct endothermic peak can be seen at 421 K in Fig. 5a, which corresponds to the phase transformation temperature (α-$Ag_2Te \rightarrow \beta$-Ag_2Te) [18]. According to the DSC plot in Fig. 5b, the latent heat of the phase transition is 29.34 J g^{-1}. This value is much different from that reported by Li (3.93 J g^{-1}) [31] but close to the calculated results of the thin film (25.75 J g^{-1}) and the bulk (23.12 J g^{-1}) of Ag_2Te [32,33].

3.2. Growth mechanism of Ag_2Te nanowires

To understand the growth mechanism of Ag_2Te nanowires prepared in an solvothermal system, the silver tellurium nanostructures at various stages of the growth process were characterized using FE-SEM. Fig. 6 shows the images of the samples that were taken from the reaction mixture after an aging time of (a) 2 h, (b) 4 h, (c) 6 h, (d) 8 h, (e) 12 h, (f) 16 h, (g) 18 h, (h) 20 h, and

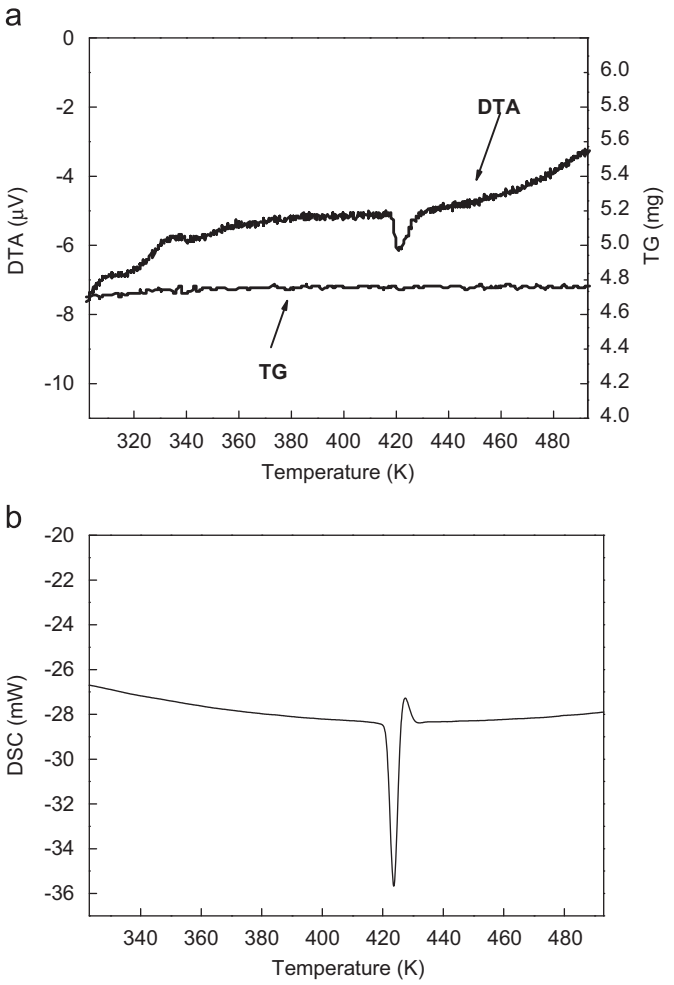

Fig. 5. (a) DTA-TG analysis and (b) DSC analysis of the Ag_2Te samples heated with 10 K/min up to 493 K.

(i) 24 h at 513 K. These images clearly show the evolution of silver tellurium nanostructures from particles into ultra-long wire-like morphology over time at 513 K. For the transformation of the nanowires, topotactic transformation mechanisms can be considered. Based on the experimental results, the formation process of ultra-long Ag_2Te wires is proposed as follows:

First of all, Ag, Te, Ag_2Te nucleation: Fig. 6a shows that the samples were comprised of numerous smaller crystallites of about 100–500 nm and we can believe that in this step, Ag phase, highly anisotropic Te phase and a little amount of Ag_2Te phase proceeded through nucleation and coexisted. To the best of our knowledge, Ag core and Te core could be easily nucleated and can be grown in EG solvents at appropriate temperature [34]. In addition, $Na_2(EDTA)\cdot 2H_2O$ and NaOH could reduce the concentration of free Ag^+ and $E_{Ag^+/Ag}$ effectively, which played a crisis role in this reduction condition.

Then, Te nanotubes and Ag_2Te wires Growth: In this step, highly anisotropic Te nanotubes can be easily and directly grown along *c*-axis from Te seeds without the use of any physical templates [34,35]. But how Te tubes transform to Ag_2Te wires? Consulting the literature, two possible mechanisms can be considered. The one is that active Ag atom in supersaturated solution adsorbed on the surface of Te nanotubes inner and outer, and then rearranged, reaction. Similarly, the copper and silver chalcogenides have been prepared by this topotactic transformation mechanism [32–35]. Another one is the split of Ag_2Te tubes and half-tubes formed by inward diffusion of Ag on surface of Te tubes, which is similar with the report of Purkayastha et al. [36] for the preparation of single-crystal lead telluride nanorods. It should be mentioned that there were some bent Ag_2Te nanowires as indicated in Fig. 6b–e because of the mechanical stress resulted from the change of atom radius and band length in the conversion of Te to Ag_2Te [26,37]. In addition, $Na_2(EDTA)\cdot 2H_2O$ could not only stabilize Ag^+ at the beginning stage, but also releases Ag^+ gradually when main reaction consume Ag phase, which was a very important factor to obtain pure samples.

Finally, Ostwald Ripening of Ag_2Te nanowires: As soon as Ag_2Te crystallites existed, there was a balance between Ag_2Te nanowires and smaller Ag_2Te crystallites. As indicated in Fig. 6f–i, Ag_2Te wires grown at the expense of the smaller ones [38] and it can be seen there is only wire-like morphology for the sample prepared for 24 h. This mechanism is totally different from the work of Qin et al. [25] and Zuo et al. [26] for the preparation of silver telluride. Furthermore, XRD and TEM results have proved that Ag_2Te phase existed in samples prepared for 8 and 16 h.

Experimental studies with X-ray diffraction for the samples that were taken from the reaction mixture after an aging time of (a) 4 h, (b) 8 h (c) 16 h, and (d) 24 h at 513 K have also provided evidence to support this proposed mechanism. In this process, the ethylene glycol could serve as both solvent and reducing reagent [34]. The XRD investigation shown in Fig. 7 indicates that all of the sample prepared in the present work can be indexed to the monoclinic Ag_2Te phase. Almost only Te phase and Ag phase could be obtained by reaction for 4 h, which can be seen in Fig. 7a. In particular, the intensity of Te crystallographic phase in the products is indeed increased gradually with the reaction time from 8 to 16 h in Fig. 7b and c which indicates that preferential orientation of Te nanotubes occurred [34]. It is easy to understand that the relative amount of Ag_2Te, Ag, and Te phase would change gradually which depended on the reaction time. Finally, pure and ultra-long Ag_2Te wires could be obtained as reaction time went to 24 h in Fig. 7d. On the basis of the experimental results, the whole process for the formation of Ag_2Te wires can be schematically illustrated in Fig. 8. In the early stage, the intermediate products indicate the coexistence of Ag particles and Te particles. As the reaction continued, it can be noted that the particles gradually disappear with the dramatical increase in the production of Te nanotubes. For the transformation process from Te nanotubes to Ag_2Te wires during 8–24 h, we can understand this interesting phenomenon by topotactic transformation.

3.3. *The electrical conductivity and Seebeck coefficient of Ag_2Te nanowires*

The thermoelectric properties of the bulk and film silver telluride have been studied by many researchers. From these studies, they have observed abrupt changes of the Hall coefficient, the Seebeck coefficient, and the electrical conductivity at 140 °C, a consequence of the structural phase transition. Fujikane et al. [39,40] have studied the thermoelectric properties of silver telluride in bulk form over a wide temperature range from 4 to 450 K. Around 150 °C, Das et al. [41] have observed the maximum Seebeck coefficient of the thin film to be $-110\ \mu V\ K^{-1}$ in the thickness of 58 nm. Gnanadurai et al. [32] have also found the maximum Seebeck coefficient of the thin film to be $130\ \mu V\ K^{-1}$ in the optimal thickness of 41 nm during the cooling process.

The temperature-dependent Seebeck coefficient of as-prepared wire-like Ag_2Te (Fig. 9a) also demonstrates the structural phase transition. The two standard error bars stands for the maximum and minimum values include the uncertainties in measuring electrical conductivity as well as Seebeck coefficient. The maximum value observed for the Seebeck coefficient (*S*)

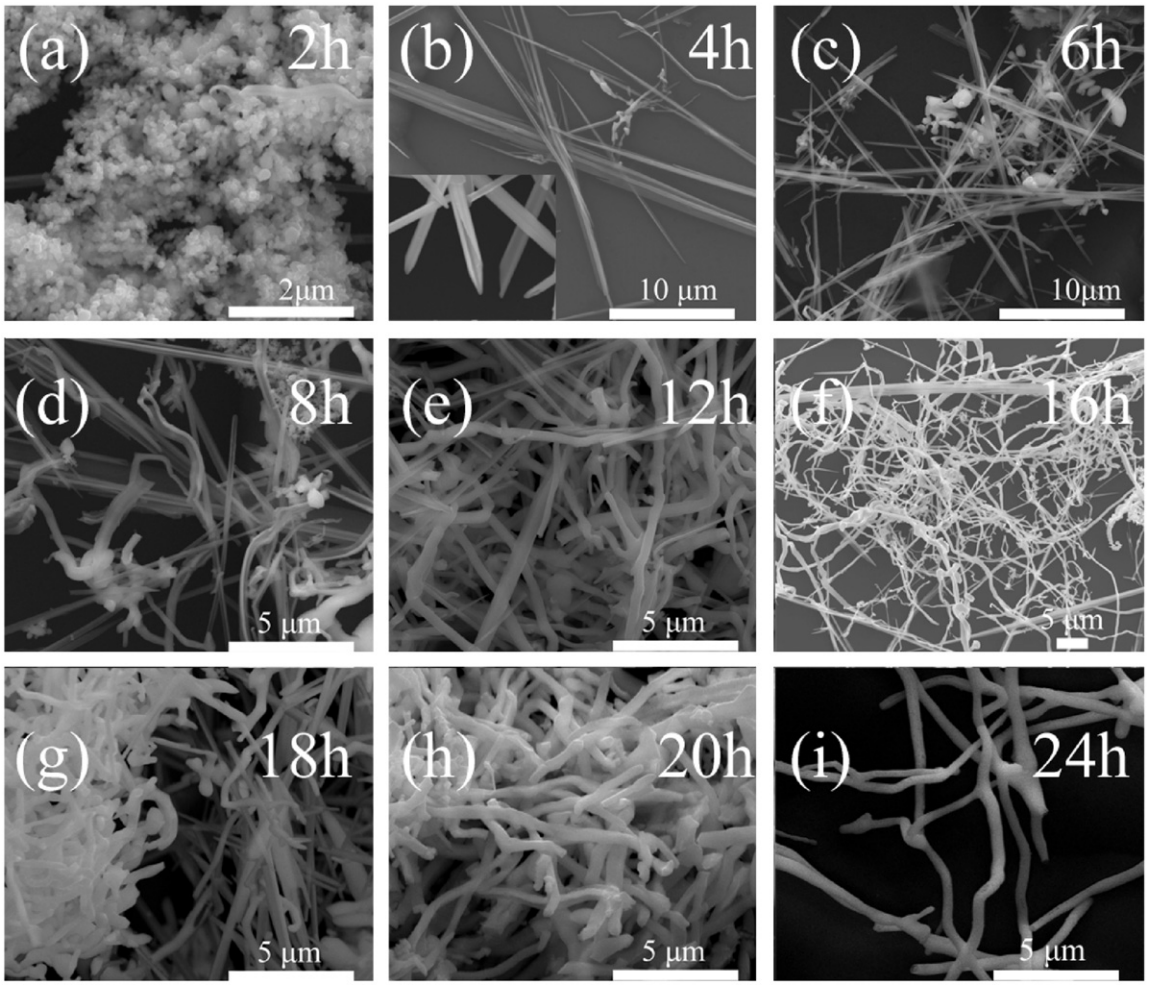

Fig. 6. FE-SEM images of the Ag_2Te samples hydrothermal treated at 513 K for (a) 2 h, (b) 4 h, (c) 6 h, (d) 8 h, (e) 12 h, (f) 16 h, (g) 18 h, (h) 20 h, and (i) 24 h.

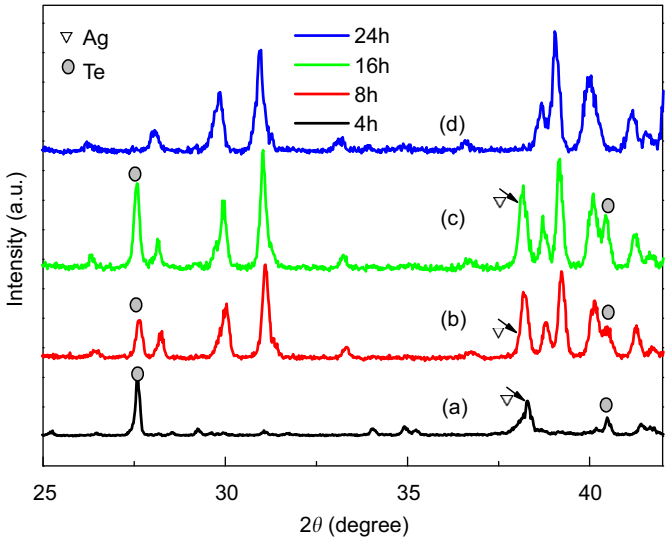

Fig. 7. The XRD patterns of the Ag_2Te samples treated hydrothermally for (a) 4 h, (b) 8 h, (c) 16 h, and (d) 24 h.

was $-70\ \mu V\ K^{-1}$, which was lower than the reported value ($-160\ \mu V\ K^{-1}$) [18]. It can be observed distinctly that the Seebeck coefficient greatly decreases at 426 K, implying that sample's structure and the carrier concentration changes greatly. Fig. 9b shows the behavior of the electrical conductivity in the temperature range of 300–673 K. The electrical conductivity increases with increasing temperature below 373 K, which is consistent with the property of semiconductor's electrical conductivity. From 373 to 423 K, the $\sigma(T)$ curve greatly decreases with increase in temperature, which indicated the structure of Ag_2Te changes greatly as results of phase transition of β-Ag_2Te to α-Ag_2Te. Then $\sigma(T)$ curve slowly increases with increase in temperature above 423 K. Because the electronic conductivity is strongly dependent on Seebeck coefficient (S) [42], it is easy to explain the abrupt decrease of the value of the electrical conductivity in the temperature range between about 373 and 423 K. The maximum value observed for the electrical conductivity σ was 30 S cm^{-1}, which was much higher than reported value (0.7 S cm^{-1}) for wire-like Ag_2Te [18]. This is possibly due to interconnection in the NW network and the length (>20 μm) of the single crystal NWs are higher than the mean free path of electron in Ag_2Te far away [43,44]. The interconnection in the NW network can reduce the interface electron scattering while ultra-long single crystal nanowires morphology can provide a good 1-D transporting channels. Further investigation is currently undergoing to verify this.

4. Conclusions

In summary, ultra-long single crystal β-Ag_2Te nanowires have been successfully synthesized by one-pot solvothermal co-reduction method at moderate temperatures and ratio of $AgNO_3$ to

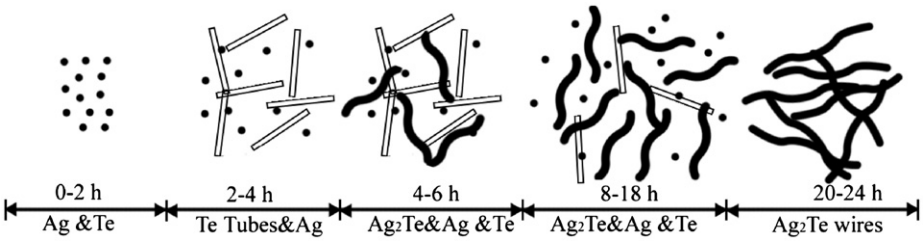

Fig. 8. Schematic representation of the formation mechanism of Ag_2Te wires. The diagram displays the variation of the phases and morphologies of products with different reaction time.

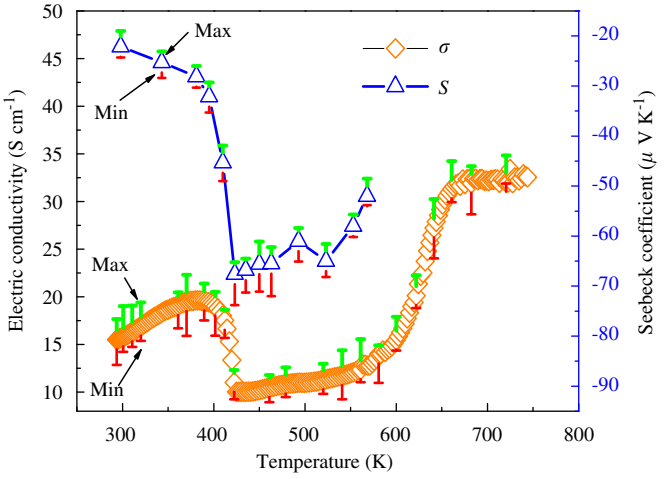

Fig. 9. (a) Temperature dependence of the Seebeck coefficient (b) Electrical conductivity for pure Ag_2Te samples. The two standard error bars include the uncertainties in measuring Seebeck coefficient and electrical conductivity.

Na_2TeO_3. The phenomenon of phase transitions of the as-prepared long wire-like Ag_2Te from monoclinic structure (β-Ag_2Te) to face-centered cubic structure (α-Ag_2Te) around 421 K are obviously observed. In our experiment, reaction time and mol ratio of $AgNO_3$ to Na_2TeO_3 were found to have more influence on the morphology of the products. Based on our experimental results, anisotropic Te nanotubes grow and transform the nanotubes into single-crystal β-Ag_2Te wires via reaction with an Ag salt.

Acknowledgment

This work was supported by the National Natural Science Foundation of China (Project no. 20871036) and the Development Program for Outstanding Young Teachers in Harbin Institute of Technology (HITQNJS.2009.001).

References

[1] T. Gandhi, K.S. Raja, I. Chatterjee, M. Misra, X. Luo, P. Dzurella, Int. J. Nanotechnol. 5 (2008) 519.
[2] X.H. Sun, B. Yu, G. Ng, M. Meyyappan, J. Phys. Chem. C 111 (2007) 2421.
[3] S. Meister, D.T. Schoen, M.A. Topinka, A.M. Minor, Y. Cui, Nano Lett. 8 (2008) 4562.
[4] W.J. Xie, X.F. Tang, Y.G. Yan, Q.J. Zhang, T.M. Tritt, J. Appl. Phys. 105 (2009) 113713.
[5] J.P. Heremans, Acta Phys. Pol. A 108 (2005) 609.
[6] M. Karlowatz, M. Kraft, B. Mizaikoff, Anal. Chem. 76 (2004) 2643.
[7] V. Venugopal, S.G. Kulkarni, A.A. Banerjee, G.A.R. Rao, K.N. Roy, D.D. Sood, J. Nucl. Mater. 238 (1996) 218.
[8] L. Bindi, J. Alloys Compd. 473 (2009) 262.
[9] Y. Izumi, S. Miyatani, J. Phys. Soc. Jpn. 35 (1973) 312.
[10] M. Gobec, W. Sitte, J. Alloys Compd. 220 (1995) 152.
[11] C. Jia, B. Zhang, W.F. Liu, C.G. Jin, L.Z. Yao, W.L. Cai, X.G. Li, J. Cryst. Growth 285 (2005) 527.
[12] Y. Sun, M.B. Salamon, M. Lee, T.F. Rosenbaum, Appl. Phys. Lett. 82 (2003) 1440.
[13] H.S. Schnyders, M.L. Saboungi, T.F. Rosenbaum, Appl. Phys. Lett. 76 (2000) 1710.
[14] A. Husmann, J.B. Betts, G.S. Boebinger, A. Migliori, T.F. Rosenbaum, M.L. Saboungi, Nature 417 (2002) 421.
[15] M. Lee, T.F. Rosenbaum, M.-L. Saboungi, H.S. Schnyders, Phys. Rev. Lett. 88 (2002) 066602.
[16] S.K. Batabyal, J.J. Vittal, Chem. Mater. 20 (2008) 5845.
[17] V.B. Prabhune, V.J. Fulari, Opt. Commun. 282 (2009) 2118.
[18] F.Y. Li, C.G. Hu, Y.F. Xiong, B.Y. Wan, W. Yan, M.C. Zhang, J. Phys. Chem. C 112 (2008) 16130.
[19] R. Dalven, R. Gill, J. Appl. Phys. 38 (1967) 753.
[20] R.Z. Chen, D.S. Xu, G.L. Guo, L.L. Gui, J. Mater. Chem. 12 (2002) 2435.
[21] R.J. Coustal, J. Chem. Phys. 38 (1958) 277.
[22] C.J. Warren, R.C. Haushalter, A.B. Bocarsly, J. Alloys Compd. 229 (1995) 175.
[23] Y. Jiang, Y. Wu, Z.P. Yang, Y. Xie, Y.T. Qian, J. Cryst. Growth 224 (2001) 1.
[24] A.K. Samal, T. Pradeep, J. Phys. Chem. C 113 (2009) 13539.
[25] A.M. Qin, Y.P. Fang, P.F. Tao, J.Y. Zhang, C.Y. Su, Inorg. Chem. 46 (2007) 7403.
[26] P.F. Zuo, S.Y. Zhang, B.K. Jin, Y.P. Tian, J.X. Yang, J. Phys. Chem. C 112 (2008) 14825.
[27] X. Wang, H.F. Wu, Q. Kuang, R.B. Huang, Z.X. Xie, L.S. Zheng, Langmuir 26 (2009) 2774.
[28] X. Ji, B. Zhang, T.M. Tritt, J.W. Kolis, A. Kumbhar, J. Electron. Mater. 36 (2007) 721.
[29] T. Gunter, A. Koberl, Electrochim. Acta 52 (2007) 2716.
[30] J.M. McLellan, A. Siekkinen, J.Y. Chen, Y.N. Xia, Chem. Phys. Lett. 427 (2006) 122.
[31] R. Venkatasubramanian, E. Siivola, T. Colpitts, B. O'Quinn, Nature 413 (2001) 597.
[32] P. Gnanadurai, N. Soundararajan, C.E. Sooriamoorthy, Vacuum 67 (2002) 275.
[33] S. Aliev, F.F. Aliev, Z.S. Gasanov, Phys. Solid State 40 (1998) 1540.
[34] B. Mayers, Y.N. Xia, Adv. Mater. 14 (2002) 279.
[35] G.C. Xi, Y.K. Liu, X.Q. Wang, X.Y. Liu, Y.Y. Peng, Y.T. Qian, Cryst. Growth Des. 6 (2006) 2567.
[36] A. Purkayastha, Q.Y. Yan, D.D. Gandhi, H.F. Li, G. Pattanaik, T. Borca-Tasciuc, N. Ravishankar, G. Ramanath, Chem. Mater. 20 (2008) 4791.
[37] G.D. Moon, S.W. Ko, Y.N. Xia, U. Jeong, ACS Nano 4 (2010) 2307.
[38] W.Z. Ostwald, Phys. Chem. 34 (1900) 495.
[39] M. Fujikane, K. Kurosaki, H. Muta, S. Yamanaka, J. Alloys Compd. 387 (2005) 297.
[40] M. Fujikane, K. Kurosaki, H. Muta, S. Yamanaka, J. Alloys Compd. 393 (2005) 299.
[41] V.D. Das, D. Karunakaran, Phys. Rev. B 30 (1984) 2036.
[42] K. Park, K.U. Jang, H.C. Kwon, J.G. Kim, W.S. Cho, J. Alloys Compd. 419 (2006) 213.
[43] Q.Y. Yan, H. Chen, W.W. Zhou, H.H. Hng, F.Y.C. Boey, J. Ma, Chem. Mater. 20 (2008) 6298.
[44] Y.P. Song, A.L. Schmitt, S. Jin, Nano Lett. 7 (2007) 965.